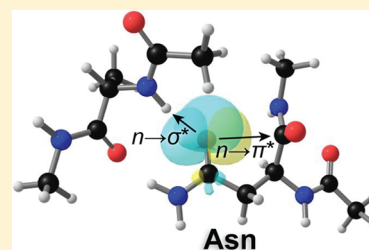


Interplay of Hydrogen Bonds and  $n \rightarrow \pi^*$  Interactions in ProteinsGail J. Bartlett,<sup>†</sup> Robert W. Newberry,<sup>‡</sup> Brett VanVeller,<sup>‡</sup> Ronald T. Raines,<sup>\*,‡,§</sup>  
and Derek N. Woolfson<sup>\*,†,||</sup><sup>†</sup>School of Chemistry, University of Bristol, Bristol BS8 1TS, United Kingdom<sup>‡</sup>Department of Chemistry and <sup>§</sup>Department of Biochemistry, University of Wisconsin-Madison, Madison, Wisconsin 53706, United States<sup>||</sup>School of Biochemistry, University of Bristol, Bristol BS8 1TD, United Kingdom

## S Supporting Information

**ABSTRACT:** Protein structures are stabilized by multiple weak interactions, including the hydrophobic effect, hydrogen bonds, electrostatic effects, and van der Waals interactions. Among these interactions, the hydrogen bond is distinct in having its origins in electron delocalization. Recently, another type of electron delocalization, the  $n \rightarrow \pi^*$  interaction between carbonyl groups, has been shown to play a role in stabilizing protein structure. Here we examine the interplay between hydrogen bonding and  $n \rightarrow \pi^*$  interactions. To address this issue, we used data available from high-resolution protein crystal structures to interrogate asparagine side-chain oxygen atoms that are both acceptors of a hydrogen bond and donors of an  $n \rightarrow \pi^*$  interaction. Then we employed natural bond orbital analysis to determine the relative energetic contributions of the hydrogen bonds and  $n \rightarrow \pi^*$  interactions in these systems. We found that an  $n \rightarrow \pi^*$  interaction is worth  $\sim 5\text{--}25\%$  of a hydrogen bond and that stronger hydrogen bonds tend to attenuate or obscure  $n \rightarrow \pi^*$  interactions. Conversely, weaker hydrogen bonds correlate with stronger  $n \rightarrow \pi^*$  interactions and demixing of the orbitals occupied by the oxygen lone pairs. Thus, these two interactions conspire to stabilize local backbone–side-chain contacts, which argues for the inclusion of  $n \rightarrow \pi^*$  interactions in the inventory of non-covalent forces that contribute to protein stability and thus in force fields for biomolecular modeling.



## ■ INTRODUCTION

Protein three-dimensional structures are the result of a fine balance of inter- and intramolecular forces, including the hydrophobic effect, van der Waals interactions, dipole effects, and hydrogen bonds.<sup>1,2</sup> Recently, it has been shown that the  $n \rightarrow \pi^*$  interaction, an electronic delocalization effect analogous to the hydrogen bond, also plays a role in stabilizing protein structure.<sup>3–6</sup> In the case of the hydrogen bond, electrons occupying the lone-pair (n) orbital of the hydrogen-bond acceptor are delocalized into the empty antibonding  $\sigma^*$  orbital of the hydrogen-bond donor.<sup>7</sup> Similarly, in an  $n \rightarrow \pi^*$  interaction, electrons from the n orbital of a carbonyl oxygen donor are delocalized into the antibonding  $\pi^*$  orbital of the carbonyl carbon acceptor, thereby drawing carbonyl groups closer together. The energy associated with an  $n \rightarrow \pi^*$  interaction between amide bonds has been estimated to contribute at least 0.27 kcal/mol.<sup>8</sup> Approximately 34% of residues in proteins are predicted to engage in  $n \rightarrow \pi^*$  interactions between backbone carbonyl groups.<sup>6</sup> It follows that  $n \rightarrow \pi^*$  interactions could provide up to 9 kcal/mol of stabilizing energy to a 100-residue protein, which, given that the free energy difference between the folded and unfolded states has been estimated to be between 5 and 10 kcal/mol for an average protein of 100 residues,<sup>9</sup> is a prodigious contribution.

Knowledge of the geometry and energetics of these weak but abundant interactions is key to a full understanding of biomolecular systems and for providing accurate force field

parameters to model them. The current challenges in *de novo* structure prediction and protein design show that our understanding of these interactions is incomplete.<sup>10,11</sup> In particular, since both hydrogen bonding and  $n \rightarrow \pi^*$  interactions involve carbonyl oxygen lone pairs, we reasoned that the presence of a hydrogen bond could affect the geometry and energy of an  $n \rightarrow \pi^*$  interaction and vice versa. For example, it has been shown that a transannular  $C_i=O \cdots H-N/O$  hydrogen bond from a 4(S)-configured NH or OH donor on a substituted proline enhances the carbonyl as an acceptor of an  $n \rightarrow \pi^*$  interaction.<sup>12–14</sup> While hydrogen-bond donation to the putative  $n \rightarrow \pi^*$  acceptor should enhance the  $n \rightarrow \pi^*$  interaction, the effect of hydrogen-bond donation to the  $n \rightarrow \pi^*$  donor is less clear. This issue is of importance for understanding the role of both hydrogen bonds and  $n \rightarrow \pi^*$  interactions. Any cooperativity or interdependence between them is likely to have an impact on protein folding, engineering, and design; structure prediction and modeling; drug design; and other aspects of chemical and structural biology.

We sought to examine the interplay between hydrogen bonds and  $n \rightarrow \pi^*$  interactions in protein structures by examining groups that could make both hydrogen bonds and  $n \rightarrow \pi^*$  interactions. Many  $n \rightarrow \pi^*$  interactions are found between sequential carbonyl groups in the protein backbone;<sup>6</sup>

Received: October 16, 2013

Published: November 20, 2013



however, these backbone atoms are under greater steric constraints than are protein side-chain atoms, which have greater conformational freedom. Hence, to study the intrinsic interplay between hydrogen bonds and  $n \rightarrow \pi^*$  interactions, we focused on protein side chains. Surveys of the Protein Data Bank (PDB)<sup>15</sup> have identified self-contacting aspartate, asparagine, glutamate, and glutamine residues in protein structures<sup>16,17</sup> and propose that they provide significant stability. Similarly, quantum-chemical calculations on self-contacting aspartic acid residues have provided evidence that these can interact via  $n \rightarrow \pi^*$  interactions.<sup>18</sup> A more recent study surveyed the side-chain–backbone hydrogen-bonded motifs formed by asparagine and glutamine in protein structures.<sup>19</sup> None of these previous studies considered hydrogen bonds and  $n \rightarrow \pi^*$  interactions together.

For our analysis, we chose to consider asparagine residues. The asparagine side-chain oxygen atom is capable of accepting a hydrogen bond from a donor and is additionally capable of donating an  $n \rightarrow \pi^*$  interaction to its main-chain carbonyl. The same is true of glutamine, but there are far fewer examples of glutamine side-chain atoms contacting the backbone,<sup>17</sup> presumably because of the entropic cost of tethering a longer methylene chain. By examining asparagine residues that make both one hydrogen bond and one  $n \rightarrow \pi^*$  interaction, we have revealed how the hydrogen bond and  $n \rightarrow \pi^*$  interaction interrelate.

## RESULTS

**Data Set Selection.** First, we identified asparagine residues from a data set of high-resolution protein structures that made single hydrogen bonds between their side-chain oxygen and the protein backbone (see Methods). We focused exclusively on backbone NH hydrogen-bond donors because (a) they provided the greatest number of examples, and (b) there was less ambiguity about hydrogen placement, making the system more amenable to electronic structure calculations. Upon inspection of this data set, we observed two common motifs and therefore divided these residues into two categories: (1) those forming a single  $\text{C}=\text{O} \cdots \text{H}-\text{N}$ ,  $i \rightarrow i+2$  hydrogen bond, commonly found at turns in protein secondary structures (for secondary structure classification, see Figure S1 in the Supporting Information), and (2) those forming a single  $\text{C}=\text{O} \cdots \text{H}-\text{N}$ ,  $i \rightarrow i+n$  hydrogen bond, where  $n > 5$ . These are shown in panels A and B of Figure 1 and are called “local” and “nonlocal” Asn groups, respectively. In addition, category (1) provided the largest number of  $n \rightarrow \pi^*$  interactions made by an asparagine side-chain residue. The numbers of Asn residues making single  $\text{C}=\text{O} \cdots \text{H}-\text{N}$ ,  $i \rightarrow i+n$  hydrogen bonds with  $n = 3-5$  were relatively small (334, 20, and 15, respectively), and the proportions of these that made  $n \rightarrow \pi^*$  interactions were too small to draw any statistically significant conclusions about the interplay between the two types of interaction. Therefore, they were excluded from the analysis.

**Parameters Defining  $n \rightarrow \pi^*$  Interactions within Asparagine residues.** Two parameters are used to define  $n \rightarrow \pi^*$  interactions between the asparagine side-chain and backbone carbonyl groups (Figure 1C): the distance between the side-chain oxygen atom and the main-chain carbonyl carbon atom ( $d_{n \rightarrow \pi^*}$ ) and the angle formed by the side-chain oxygen atom, the main-chain carbonyl carbon atom, and the main-chain oxygen atom ( $\theta$ ). For the work presented herein, these parameters were used to give an operational definition of  $n \rightarrow \pi^*$  interactions:  $d_{n \rightarrow \pi^*} \leq 3.22 \text{ \AA}$  (the sum of the van der Waals radii

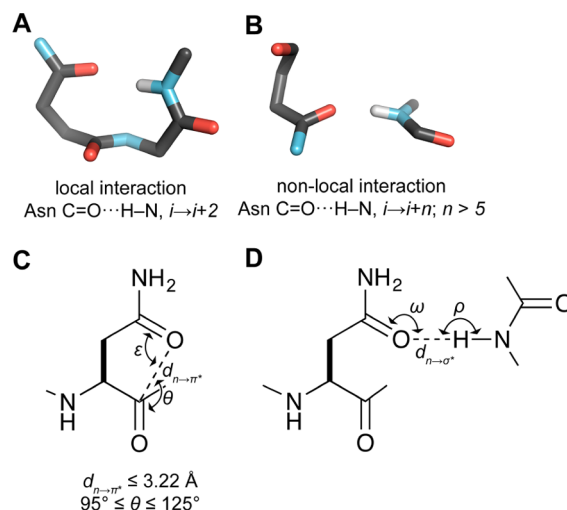


**Figure 1.** Definition of (A) local and (B) nonlocal asparagine side-chain hydrogen bonds. Parameters defining (C)  $n \rightarrow \pi^*$  interactions and (D) hydrogen bonds in an asparagine side-chain system.

of oxygen and carbon) and  $95^\circ \leq \theta \leq 125^\circ$  (a range centered on the approximate angle of the Bürgi–Dunitz trajectory for nucleophilic attack at a carbonyl carbon,  $\sim 109^\circ$ ). In addition, the angle  $\varepsilon$  formed by the side-chain carbonyl carbon, the side-chain carbonyl oxygen, and the main-chain carbonyl carbon was recorded. This angle should approach  $90^\circ$  when complete demixing of the lone-pair orbitals on the donor oxygen occurs.

**Parameters Defining Hydrogen Bonds.** The relevant hydrogen-bond parameters (Figure 1D) are  $d_{n \rightarrow \sigma^*}$ , the distance between the side-chain oxygen and backbone nitrogen atoms, and the angle  $\omega$  formed by the side-chain carbonyl carbon, the side-chain carbonyl oxygen, and the donor hydrogen atom. We also recorded the angle  $\rho$  between the hydrogen-bond donor and acceptor. This angle is a measure of hydrogen-bond ideality, which tends toward  $180^\circ$  for an optimal hydrogen bond. Inspection of the hydrogen-bond  $\rho$  parameters for both Asn groups (Figure 2B,D) showed that they are nonideal, even in the nonlocal case, where steric restrictions should be at a minimum.

### Hydrogen-Bond Geometries of Asparagine Residues.

We found 823 Asn residues that make a local  $\text{Asn C}=\text{O} \cdots \text{H}-\text{N}$ ,  $i \rightarrow i+2$  hydrogen bond in our data set. The local Asn group was characterized by  $\omega$  angles of  $\sim 140^\circ$  and  $\rho$  angles of  $\sim 165^\circ$  (Figure 2A). Those Asn residues making  $n \rightarrow \pi^*$  interactions had a slightly higher average  $\omega$  but a similar distribution of  $\rho$ . We found 972 Asn residues that make a nonlocal  $\text{Asn C}=\text{O} \cdots \text{H}-\text{N}$ ,  $i \rightarrow i+n$  ( $n > 5$ ) hydrogen bond in our data set. This group had a slightly flatter distribution of  $\omega$  with a mean of  $\sim 125^\circ$ , and the distribution of  $\rho$  was slightly shifted more toward linear hydrogen bonds (Figure 2B). In both groups, the distribution of  $\omega$  values was shifted to higher values than those found previously,<sup>20</sup> with greater distortions observed in the local case. This shift could be because the previous study did not fully account for residues accepting multiple hydrogen bonds from different donors, whereas the present study does take this into consideration. This distinction could be significant—force fields derived from previous studies<sup>21</sup> have been used successfully in protein design,<sup>22–24</sup> but two recent perspectives highlight difficulties with the treatment of the hydrogen bond.<sup>11,25</sup> Specifically, the energy term for side-chain–backbone hydrogen bonds is derived from statistics for

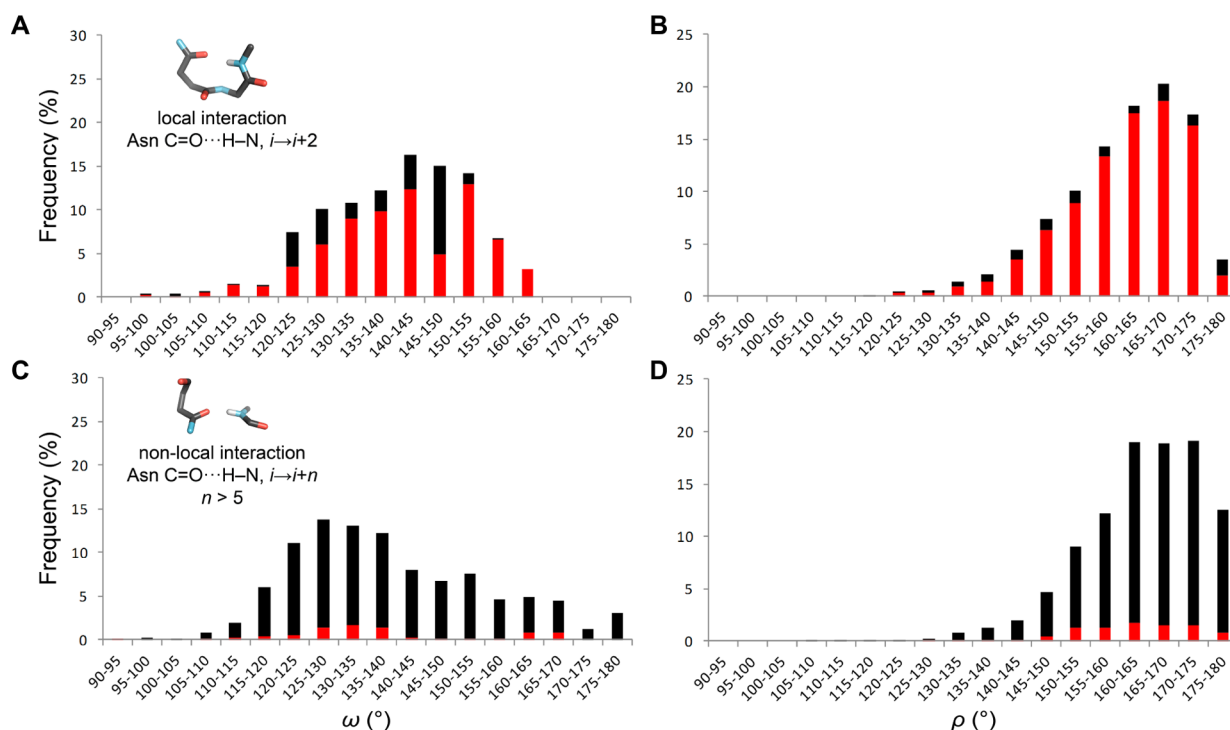


**Figure 2.** Histograms of hydrogen-bond geometry parameters in the (A, B) local and (C, D) nonlocal Asn groups. The frequency in each bin was corrected by  $1/\sin(\omega)$  or  $1/\sin(\rho)$  and then normalized so the local and nonlocal groups can be compared. Red indicates residues testing positive for an  $n \rightarrow \pi^*$  interaction according to the operational definition in Figure 1C. The height of the red bar indicates the corrected, normalized proportion of the bin making an  $n \rightarrow \pi^*$  interaction with the backbone carbonyl group. The means (standard deviations) of the underlying distributions are as follows: (A)  $n \rightarrow \pi^*$ -positive 139.2 (12.0),  $n \rightarrow \pi^*$ -negative 133.2 (12.0); (B)  $n \rightarrow \pi^*$ -positive 156.7 (10.7),  $n \rightarrow \pi^*$ -negative 149.2 (14.1); (C)  $n \rightarrow \pi^*$ -positive 131.4 (13.5),  $n \rightarrow \pi^*$ -negative 133.9 (13.5); (D)  $n \rightarrow \pi^*$ -positive 158.0 (9.7),  $n \rightarrow \pi^*$ -negative 158.7 (10.9).

side-chain–side-chain hydrogen bonds; in our data set, we observed significant deviation from this paradigm, suggesting that design efforts could be improved by better accounting for side-chain–backbone hydrogen-bond geometries, at least for asparagine residues.

**Dependence of  $n \rightarrow \pi^*$  Interactions on the Hydrogen-Bond Environment.** We found 725  $n \rightarrow \pi^*$  interactions where the Asn also makes a local hydrogen bond. Those interactions represent a much larger proportion than the 92  $n \rightarrow \pi^*$  interactions found where the hydrogen bond is a nonlocal interaction (88% local versus 9.5% nonlocal hydrogen bonds). Nonlocal hydrogen bonds likely “distract” the Asn side chain from making a local  $n \rightarrow \pi^*$  interaction, suggesting that hydrogen bonds form preferentially to  $n \rightarrow \pi^*$  interactions, which we believe is consistent with their relative energies. In this case, hydrogen bonds can form with a more typical geometry (i.e.,  $\omega \approx 120^\circ$ ) relative to the local case. Intrigued by the correlation of  $n \rightarrow \pi^*$  prevalence and the atypical hydrogen-bond geometry in local Asn contacts, we examined how the geometry of the hydrogen bond affects the geometry of the  $n \rightarrow \pi^*$  interaction.

There is a relationship between  $\epsilon$  and  $\omega$  for the local Asn group (Figure 3A). As the hydrogen bond becomes more linear (i.e.,  $\omega$  tends to  $180^\circ$ ), the angle made by the donor  $C=O$  group and its acceptor carbonyl carbon,  $\epsilon$ , tends to  $90^\circ$ . This trend, which is not observed in the nonlocal Asn group (Figure 3B), could indicate orbital demixing in the case of the local-side-chain Asn residues making  $n \rightarrow \pi^*$  interactions.

**Computational Analyses.** We probed the relationship between  $\epsilon$  and  $\omega$  further. Specifically, we carried out natural bond orbital (NBO) calculations on a subset of local and

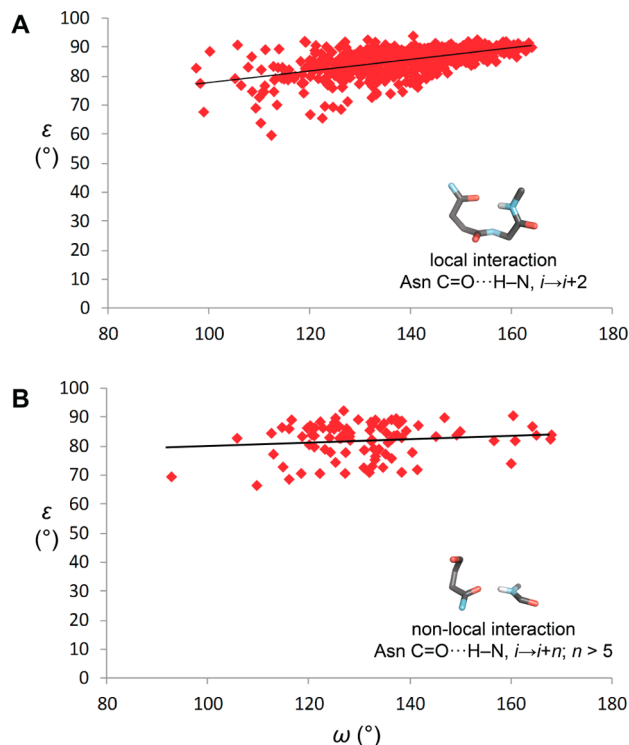


**Figure 3.** Scatter plot of hydrogen-bond angle  $\omega$  versus  $n \rightarrow \pi^*$  interaction angle  $\epsilon$  for  $n \rightarrow \pi^*$ -positive residues in the (A) local and (B) nonlocal Asn groups. The black lines are from linear least-squares fits (local  $R^2 = 0.32$ ; nonlocal  $R^2 = 0.03$ ).

nonlocal Asn residues and their hydrogen-bond donors in order to estimate the energy contributed to both the  $n \rightarrow \pi^*$  interaction and the hydrogen bond ( $n \rightarrow \sigma^*$  interaction) by the Asn side-chain carbonyl group. We restricted our NBO analysis to only the participating functional groups in vacuum, (i.e., with a dielectric constant of 1; see Methods). Thus, we comment exclusively on relative energies associated with hydrogen bonds and  $n \rightarrow \pi^*$  interactions and not their absolute magnitudes. We found, unsurprisingly, that hydrogen bonds were stronger than  $n \rightarrow \pi^*$  interactions. In our calculations, an  $n \rightarrow \pi^*$  interaction was worth anywhere between 6% and 23% of the competing hydrogen bond (Table 1). The hydrogen bond was also preferred to the  $n \rightarrow \pi^*$  interaction. In the nonlocal hydrogen bonds, an average of  $(92 \pm 8)\%$  of the total

**Table 1. Average Energies (SDs) of the Hydrogen Bond ( $E_{n \rightarrow \sigma^*}$ ) and  $n \rightarrow \pi^*$  Interaction ( $E_{n \rightarrow \pi^*}$ ) in the Local and Nonlocal Asn Groups<sup>a</sup>**

	local ( $n = 26$ )	nonlocal ( $n = 47$ )
$E_{n \rightarrow \sigma^*}$ (kcal/mol)	5.37 (3.51)	10.27 (4.71)
$E_{n \rightarrow \pi^*}$ (kcal/mol)	1.23 (0.49)	0.71 (0.55)

<sup>a</sup>Differences are statistically significant ( $p < 0.05$ ).

stabilization afforded to either the antibonding  $\pi^*$  or  $\sigma^*$  orbital went to the antibonding  $\sigma^*$  orbital. In the case of the local hydrogen bonds, the  $\sigma^*$  orbital was slightly less favored, as this average was only  $(78 \pm 11)\%$ . We examined the relationship between the hydrogen-bond parameters and  $E_{n \rightarrow \sigma^*}$  and between

the  $n \rightarrow \pi^*$  interaction parameters and  $E_{n \rightarrow \pi^*}$ , as calculated with NBO analysis (Figure 4). As anticipated, in the local Asn group, as  $\omega$  tended to  $180^\circ$ ,  $E_{n \rightarrow \sigma^*}$  increased, while as  $\epsilon$  tended to  $90^\circ$  degrees,  $E_{n \rightarrow \pi^*}$  increased, similar to the trend observed from the PDB in Figure 3A. In nonlocal cases, this trend held for  $\epsilon$  but not for the hydrogen bond, which showed no preferred  $\omega$  for high values of  $E_{n \rightarrow \sigma^*}$ . In both cases, the stabilization was at its greatest when the distances  $d_{n \rightarrow \sigma^*}$  and  $d_{n \rightarrow \pi^*}$  were smallest, that is, when the orbital overlap was greatest.

We noted some differences between the local and nonlocal Asn residues. Hydrogen bonds in the nonlocal Asn group were worth almost double the energy compared with the local Asn group, whereas the  $n \rightarrow \pi^*$  interaction was worth about half the energy in the nonlocal set compared with the local set. The weakness of the hydrogen bonds observed in local contacts is consistent with the less-ideal geometry apparent in our survey of protein structures for these residues. In the presence of these weaker hydrogen bonds, however, there was a corresponding increase in the strength of the  $n \rightarrow \pi^*$  interaction. To investigate the propensity of these weaker, less-ideal hydrogen bonds to enable  $n \rightarrow \pi^*$  interactions, we examined the contributions of individual carbonyl lone pairs to both hydrogen bonds and  $n \rightarrow \pi^*$  interactions.

In the nonlocal Asn group, both lone pairs made a large contribution to the antibonding  $\sigma^*$  orbital but a small one to the antibonding  $\pi^*$  orbital, pointing toward orbital hybridization on the carbonyl oxygen (Table 2 and Figure 5). By contrast, in the local Asn group, it was apparent that orbital demixing took place: electrons from the first lone pair (LP1,

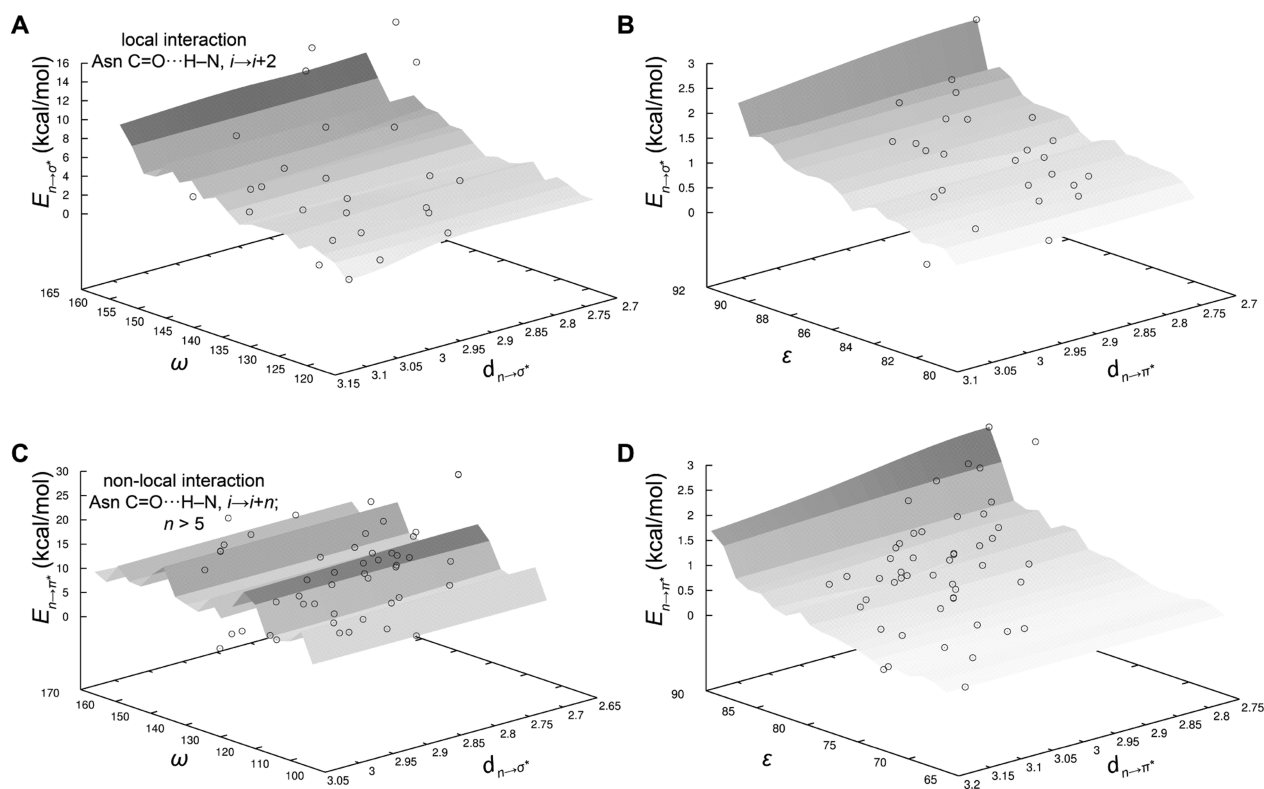


**Figure 4.** 3D plots of (A, C) hydrogen-bond energies and (B, D)  $n \rightarrow \pi^*$  interaction energies for (A, B) local and (C, D) nonlocal Asn groups. The parameters are defined in Figure 1C,D. Energies were calculated from second-order perturbation theory analysis (as implemented in NBO 3.1) of 26 examples for the local group and 47 examples for the nonlocal group. The surface was generated as a grid with dimensions of the scattered data and an arbitrarily chosen set of rows and columns that were equally spaced across the grid. The  $z$  value of the grid was computed as a weighted average of the  $z$  values of the scattered points. In addition, raw data points are plotted on top of the surface.



**Table 2.** Average Proportions of Energy Stabilization Afforded to the Hydrogen Bond ( $P_{n \rightarrow \sigma^*}$ ) and the  $n \rightarrow \pi^*$  Interaction ( $P_{n \rightarrow \pi^*}$ ) by Each Lone Pair for the Local and Nonlocal Asn Groups

	local		nonlocal	
	$P_{n \rightarrow \sigma^*}$	$P_{n \rightarrow \pi^*}$	$P_{n \rightarrow \sigma^*}$	$P_{n \rightarrow \pi^*}$
lone pair 1 (LP1)	0.930	0.070	0.959	0.040
lone pair 2 (LP2)	0.439	0.561	0.822	0.178

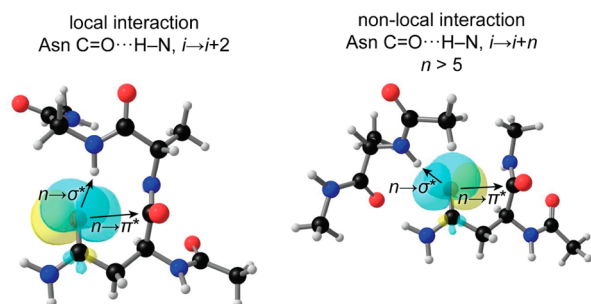


**Figure 5.** Lone-pair orbitals on the asparagine side-chain oxygen for (left) an asparagine making a local hydrogen bond (PDB 3KS3, residues 61–63) and (right) an asparagine making a nonlocal hydrogen bond (PDB 2CXA, residues 24 and 62). Values for  $E_{n \rightarrow \pi^*}$  and  $E_{n \rightarrow \sigma^*}$  as calculated with NBO analysis: (left)  $E_{n \rightarrow \pi^*} = 2.7$  kcal/mol (5% LP1, 51% LP2),  $E_{n \rightarrow \sigma^*} = 10.3$  kcal/mol (95% LP1, 49% LP2); (right)  $E_{n \rightarrow \pi^*} = 2.3$  kcal/mol (9% LP1, 16% LP2),  $E_{n \rightarrow \sigma^*} = 14.6$  kcal/mol (91% LP1, 84% LP2). Orbital images were generated with Chemcraft.

which occupies a predominantly  $s$ -type orbital) provided the most stabilization to the hydrogen bond and hardly any to the  $n \rightarrow \pi^*$  interaction. The second lone pair (LP2), which occupies a predominantly  $p$ -type orbital, provided about half its energy to the  $n \rightarrow \pi^*$  interaction and half to the hydrogen bond. A clear separation between lone-pair contributions can be seen for the local Asn group (Figure 6A), but by contrast, there was no segregation in lone-pair contributions for the nonlocal Asn group. Again, this distinction indicates orbital hybridization in the nonlocal group and orbital demixing for the local group.

These calculations were carried out in the gas phase. One might expect water to be the most forbidding solvent for both hydrogen bonds and  $n \rightarrow \pi^*$  interactions because of its ability to compete for relevant orbitals. However, while hydrogen bonding is sensitive to the dielectric constant of the medium, the strength of an  $n \rightarrow \pi^*$  interaction has been found to change only slightly in different solvents.<sup>3,26</sup> Taken together, these points suggest that the interplay observed in our calculations would likely be amplified in water, as hydrogen bonds may be weaker and the overall contribution from  $n \rightarrow \pi^*$  interactions may be increased.

## DISCUSSION

The canonical angle at which lone pairs of electrons protrude from a carbonyl oxygen to make a hydrogen bond is  $120^\circ$ .<sup>27</sup> This angle can arise from two  $sp^2$ -hybridized orbitals sitting like “rabbit ears” on the carbonyl oxygen. In their analysis of the PDB, Baker and co-workers showed that the preferred angle for hydrogen-bonded side-chain carbonyl groups is in fact  $\sim 120^\circ$ .<sup>20</sup> Indeed, in the absence of local constraints, we have observed a tendency of Asn side-chain carbonyl groups to form strong, typical (i.e.,  $\omega \approx 120^\circ$ ) hydrogen bonds with the peptide main

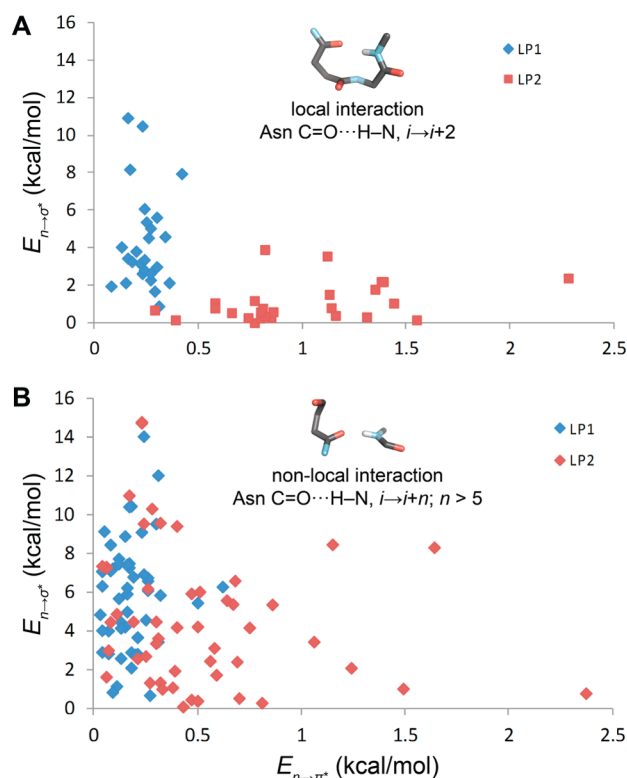


**Figure 6.** Scatter plots of  $E_{n \rightarrow \pi^*}$  vs  $E_{n \rightarrow \sigma^*}$  for individual lone pairs (LP1 = blue, LP2 = red) as assigned by using NBO analysis for (A) local and (B) nonlocal Asn groups.

chain. These hydrogen bonds reduce the prevalence of  $n \rightarrow \pi^*$  interactions involving these residues and attenuate the resulting energy of the observed  $n \rightarrow \pi^*$  interactions. In these cases, the hydrogen bond tends to obscure the  $n \rightarrow \pi^*$  interaction, and we can therefore expect the effects of  $n \rightarrow \pi^*$  interactions to be relatively low.

In the presence of local constraints imposed by the global folding of the peptide chain, however, the typical geometry of the hydrogen bond is compromised significantly, with a concomitant reduction in the hydrogen-bond energy. The geometry of these hydrogen bonds is consistent with orbital demixing and, by extension, allows enhanced  $n \rightarrow \pi^*$  interactions. As a result,  $n \rightarrow \pi^*$  interactions in the presence of local hydrogen-bond constraints are both more prevalent and of significantly higher energy. These stronger  $n \rightarrow \pi^*$  interactions seem to compensate for the weaker hydrogen bonds, allowing for side-chain–backbone contacts that might not be observed otherwise. Moreover, an extreme hydrogen-bonding angle occurs in the backbone of the  $\alpha$ -helix, where the  $C=O \cdots H-N$ ,  $i \rightarrow i+4$  hydrogen bond is found at  $\sim 160^\circ$ . We argue that this angle is associated with orbital demixing, where the hydrogen bond draws on electrons in the  $n_s$ -type orbital<sup>4</sup> that protrudes out from the carbonyl oxygen atom along the direction of the  $C=O$  bond (Figure 5). The ensuing liberation of the electrons in an  $n_p$ -type orbital<sup>4</sup> enables the  $n \rightarrow \pi^*$  interaction and thereby provides additional stability to the  $\alpha$ -helix.

These results also have implications for the parametrization of hydrogen bonds in different local environments in protein structures. Previously, side-chain–backbone hydrogen-bond energies have been derived from the statistics for side-chain–side-chain hydrogen bonds.<sup>20</sup> The different angle preferences for the hydrogen bonds accepted by Asn in different

environments are indicative of the need for a more environment-sensitive hydrogen-bond potential in molecular modeling. Additionally, we urge the inclusion of  $n \rightarrow \pi^*$  interactions in molecular-modeling force fields. We have shown previously that  $n \rightarrow \pi^*$  interactions are prevalent between sequential backbone carbonyl groups in a protein sequence, particularly in  $\alpha$ -helices.<sup>6</sup> In the Rosetta force field, for example, if a backbone–backbone hydrogen bond is made, neither the donor nor acceptor residue is allowed to participate in a backbone–side-chain hydrogen bond.<sup>28</sup> Addition of an  $n \rightarrow \pi^*$  contribution here, especially in an  $\alpha$ -helix, should improve computational accuracy. For example, a 20-residue helix could contain 16 backbone hydrogen bonds and 19 sequential backbone carbonyl  $n \rightarrow \pi^*$  interactions. If each  $n \rightarrow \pi^*$  interaction were worth 15% of a hydrogen bond, inclusion of an  $n \rightarrow \pi^*$  interaction term would provide helix stabilization equivalent to approximately three extra hydrogen bonds. Thus, although the contribution of each  $n \rightarrow \pi^*$  interaction is small in energetic terms ( $\sim 5$ – $25\%$  of a hydrogen bond), the sheer quantity of them in protein structures suggests that they are of importance.

## METHODS

**Structural Data Set.** A data set of 2540 protein X-ray crystal structures was culled from the Protein Data Bank using the PISCES server<sup>29</sup> (resolution  $\leq 1.6$  Å,  $R$  factor  $< 0.3$ , each comprising a protein chain of  $\geq 40$  residues, with  $\leq 40\%$  sequence identity between any two structures). Hydrogen bonds were assigned using HBPlus<sup>30</sup> with standard settings, except that asparagine side chains were allowed to flip according to hydrogen-bond assignment. Hydrogen bonds were assigned between defined donor (D) and acceptor [carbonyl oxygen (O)] atoms meeting the following distance and angle criteria:  $D \cdots H \cdots O$  angle  $\geq 90^\circ$ ,  $H \cdots O \cdots C$  angle  $\geq 90^\circ$ ,  $D \cdots O \cdots C$  angle  $\geq 90^\circ$ ,  $D \cdots O$  distance  $\leq 3.9$  Å, and  $H \cdots O$  distance  $\leq 2.5$  Å, with at least three covalent bonds between the donor and acceptor.<sup>31</sup> Scripts were written in Perl to identify a set of 2839 asparagine residues accepting exactly one hydrogen bond. Residues making any hydrogen bonds to water were ignored. Secondary structure parameters were calculated using the modified Kabsch and Sander method<sup>32</sup> as implemented in Promotif.<sup>33</sup>

**NBO Calculations.** A subset of the asparagine residues and their hydrogen-bond donors identified from the PDB were chosen for NBO calculations (Figure S2 in the Supporting Information).<sup>34</sup> For the local Asn group, a set was chosen that had values of the  $\epsilon$  and  $\omega$  parameters on the least-squares-fitted line shown in Figure 3A. For the nonlocal group, a set was chosen manually that sampled a widespread of  $\omega$  values. The coordinates of the asparagine residue, hydrogen-bond donor residue, and one residue on either side were extracted from the PDB file. All other residues were truncated to alanine, and the N and C termini were acetylated and amidated, respectively. We employed density functional theory (DFT) calculations at the B3LYP/6-311++G(2d,p) level with NBO analysis using second-order perturbation theory to estimate the contributions of the lone pairs on the asparagine side-chain oxygen to the  $n \rightarrow \pi^*$  interaction ( $E_{n \rightarrow \pi^*}$ ) and  $n \rightarrow \sigma^*$  interaction (hydrogen bond,  $E_{n \rightarrow \sigma^*}$ ). DFT calculations were carried out with NBO 3.1<sup>35</sup> as implemented in Gaussian 09.<sup>36</sup>

## ASSOCIATED CONTENT

### Supporting Information

Additional figures describing secondary structure classification of local and nonlocal Asn groups and selection of Asn examples for NBO calculations; archive files providing all input coordinates in Gaussian format for NBO calculations; and data used for the analysis presented herein. This material is available free of charge via the Internet at <http://pubs.acs.org>.

## AUTHOR INFORMATION

### Corresponding Authors

rtraines@wisc.edu  
d.n.woolfson@bristol.ac.uk

### Notes

The authors declare no competing financial interest.

## ACKNOWLEDGMENTS

This work was supported by a joint grant to D.N.W. and R.T.R., EP/J001430 (EPSRC) and CHE-1124944 (NSF). Additional support was provided by Grant R01 AR044276 (NIH). R.W.N. was supported by Biotechnology Training Grant T32 GM008349 (NIH). B.V. was supported by a postdoctoral fellowship from CHIR (289613).

## REFERENCES

- (1) Anfinsen, C. B. *Science* **1973**, *181*, 223.
- (2) Dill, K. *Biochemistry* **1990**, *29*, 7133.
- (3) Hinderaker, M. P.; Raines, R. T. *Protein Sci.* **2003**, *12*, 1188.
- (4) Choudhary, A.; Raines, R. T. *Protein Sci.* **2011**, *20*, 1077.
- (5) Raines, R. T.; Choudhary, A.; Gandla, D.; Krow, G. R. *J. Am. Chem. Soc.* **2009**, *131*, 7244.
- (6) Bartlett, G. J.; Choudhary, A.; Raines, R. T.; Woolfson, D. N. *Nat. Chem. Biol.* **2010**, *6*, 615.
- (7) Alabugin, I. V.; Manoharan, M.; Peabody, S.; Weinhold, F. *J. Am. Chem. Soc.* **2003**, *125*, 5973.
- (8) Newberry, R. W.; VanVeller, B.; Guzei, I.; Raines, R. T. *J. Am. Chem. Soc.* **2013**, *135*, 7843.
- (9) Creighton, T. E. *Proteins: Structures and Molecular Properties*; 2nd ed.; Freeman: New York, 1993.
- (10) Der, B.; Jha, R. *Proteins* **2013**, *81*, 1245.
- (11) Stranges, P. B.; Kuhlman, B. *Protein Sci.* **2013**, *22*, 74.
- (12) Shoulders, M. D.; Kotch, F. W.; Choudhary, A.; Guzei, I. A.; Raines, R. T. *J. Am. Chem. Soc.* **2010**, *132*, 10857.
- (13) Erdmann, R. S.; Wennemers, H. *Angew. Chem., Int. Ed.* **2011**, *50*, 6835.
- (14) Erdmann, R. S.; Wennemers, H. *J. Am. Chem. Soc.* **2012**, *134*, 17117.
- (15) Berman, H. M.; Westbrook, J.; Feng, Z.; Gilliland, G.; Bhat, T. N.; Weissig, H.; Shindyalov, I. N.; Bourne, P. E. *Nucleic Acids Res.* **2000**, *28*, 235.
- (16) Deane, C. M.; Allen, F. H.; Taylor, R.; Blundell, T. L. *Protein Eng.* **1999**, *12*, 1025.
- (17) Pal, T. K.; Sankaramakrishnan, R. *J. Mol. Graphics Modell.* **2008**, *27*, 20.
- (18) Pal, T. K.; Sankaramakrishnan, R. *J. Phys. Chem. B* **2010**, *114*, 1038.
- (19) Vasudev, P. G.; Banerjee, M.; Ramakrishnan, C.; Balaram, P. *Proteins* **2012**, *80*, 991.
- (20) Morozov, A. V.; Kortemme, T.; Tsemekhman, K.; Baker, D. *Proc. Natl. Acad. Sci. U.S.A.* **2004**, *101*, 6946.
- (21) Baker, D.; Kortemme, T.; Morozov, A. V. *J. Mol. Biol.* **2003**, *326*, 1239.
- (22) Kuhlman, B.; Dantas, G.; Ireton, G. C.; Varani, G.; Stoddard, B. L.; Baker, D. *Science* **2003**, *302*, 1364.
- (23) Röthlisberger, D.; Khersonsky, O.; Wollacott, A. M.; Jiang, L.; DeChancie, J.; Betker, J.; Gallaher, J. L.; Althoff, E.; Zanghellini, A.; Dym, O.; Albeck, S.; Houk, K. N.; Tawfik, D. S.; Baker, D. *Nature* **2008**, *453*, 190.
- (24) Jiang, L.; Althoff, E.; Clemente, F. R.; Doyle, L.; Röthlisberger, D.; Zanghellini, A.; Gallaher, J. L.; Betker, J. L.; Tanaka, F.; Barbas, C. F., III; Hilvert, D.; Houk, K. N.; Stoddard, B. L.; Baker, D. *Science* **2008**, *319*, 1387.
- (25) Das, R. *PLoS One* **2011**, *6*, No. e20044.
- (26) Gorske, B. C.; Stringer, J. R.; Bastian, B. L.; Fowler, S. A.; Blackwell, H. E. *J. Am. Chem. Soc.* **2009**, *131*, 16555.
- (27) Gillespie, R. J.; Robinson, E. A. *Chem. Soc. Rev.* **2005**, *34*, 396.

- (28) O'Meara, M. Hydrogen Bond Energy Term. [https://www.rosettacommons.org/manuals/archive/rosetta3.5\\_user\\_guide/db/daf/hbonds.html](https://www.rosettacommons.org/manuals/archive/rosetta3.5_user_guide/db/daf/hbonds.html) (accessed Nov 22, 2013).
- (29) Wang, G.; Dunbrack, R. L. *Bioinformatics* **2003**, *19*, 1589.
- (30) McDonald, I.; Thornton, J. *J. Mol. Biol.* **1994**, *238*, 777.
- (31) Baker, E. N.; Hubbard, R. E. *Prog. Biophys. Mol. Biol.* **1984**, *44*, 97.
- (32) Kabsch, W.; Sander, C. *Biopolymers* **1983**, *22*, 2577.
- (33) Hutchinson, E.; Thornton, J. *Protein Sci.* **1996**, *5*, 212.
- (34) Reed, A. E.; Curtiss, L.; Weinhold, F. *Chem. Rev.* **1988**, *88*, 899.
- (35) Glendening, E. D.; Reed, A. E.; Carpenter, J. E.; Weinhold, F. *NBO*, version 3.1.
- (36) Frisch, M. J.; Trucks, G. W.; Schlegel, H. B.; Scuseria, G. E.; Robb, M. A.; Cheeseman, J. R.; Scalmani, G.; Barone, V.; Mennucci, B.; Petersson, G. A.; Nakatsuji, H.; Caricato, M.; Li, X.; Hratchian, H. P.; Izmaylov, A. F.; Bloino, J.; Zheng, G.; Sonnenberg, J. L.; Hada, M.; Ehara, M.; Toyota, K.; Fukuda, R.; Hasegawa, J.; Ishida, M.; Nakajima, T.; Honda, Y.; Kitao, O.; Nakai, H.; Vreven, T.; Montgomery, J. A., Jr.; Peralta, J. E.; Ogliaro, F.; Bearpark, M.; Heyd, J. J.; Brothers, E.; Kudin, K. N.; Staroverov, V. N.; Kobayashi, R.; Normand, J.; Raghavachari, K.; Rendell, A.; Burant, J. C.; Iyengar, S. S.; Tomasi, J.; Cossi, M.; Rega, N.; Millam, J. M.; Klene, M.; Knox, J. E.; Cross, J. B.; Bakken, V.; Adamo, C.; Jaramillo, J.; Gomperts, R.; Stratmann, R. E.; Yazyev, O.; Austin, A. J.; Cammi, R.; Pomelli, C.; Ochterski, J. W.; Martin, R. L.; Morokuma, K.; Zakrzewski, V. G.; Voth, G. A.; Salvador, P.; Dannenberg, J. J.; Dapprich, S.; Daniels, A. D.; Farkas, Ö.; Foresman, J. B.; Ortiz, J. V.; Cioslowski, J.; Fox, D. J. *Gaussian 09*, revision B.01; Gaussian, Inc.: Wallingford, CT, 2009.